

A Theory for the RF Surface For Metals at the Destructive Breakdown Limit

*Perry Wilson
SLAC*

By destructive breakdown we mean a breakdown event that results in surface melting over a macroscopic area in a high E-field region. A plasma forms over the molten area, bombarding the surface with an intense ion current ($\sim 10^8 \text{A/cm}^2$), which is equivalent to a pressure of about a thousand Atmospheres. This pressure causes molten copper to migrate away from the high-pressure region near the iris tip, resulting in a measurable change in the iris shape.

The four Stages of breakdown

- 1. The formation of plasma spots and individual craters in high field regions on the metal surface.**
- 2. Setting up the conditions for surface melting—crater clustering.**
- 3. Prediction for the surface field at the threshold for destructive breakdown.**
- 4. From surface melting to destructive breakdown.**

1. The Formation of Plasma Spots and Individual Craters

Formation of plasma spots during initial processing

As the gradient in a “virgin” accelerator structure is increased, sharp geometrical features in a high field region will begin to field-emit. At some field level, the tip of the projection will literally explode, injecting a jet of liquid metal vapor into the field above the projection. Field emission current quickly ionizes the vapor, leading to the formation of a plasma at the emitter site with a diameter on the order of a few microns. The plasma forms a Debye sheath at the point of contact with the metal. The sheath is a space charge limited Child’s law diode, injecting electrons into the plasma and bombarding the surface below with an intense ion counter-current on the order of 10^8 A/cm², causing the metal below the spot to melt on a sub-nanosecond time scale. The molten area and associated plasma expand until the plasma quenches after some tens of nanoseconds. A small crater-like feature, with a diameter $\sim 5\text{--}20$ μm is left behind. Plasma spots form on metal surfaces in both rf and dc fields. The craters left behind are indistinguishable in the two cases.

The energy going into the formation of a crater is very small—only about 10^{-5} J. However, the electrons injected into the vacuum by a plasma spot (~ 10 A) pick up, on the average, perhaps one hundred keV of energy from the rf field. The energy extracted from the field in 10 ns is then on the order of 0.01 J. This is sufficient to collapse the field in a cell of a typical SW structure. However, in a

TW structure energy flows into the cell at a higher rate and the rate of energy extraction by a single plasma spot is not sufficient to produce field collapse. Multiple closely spaced plasma spots can also form that extract more energy from the field.

Some possible triggers for plasma spot formation

Two models for plasma spot initiation have been investigated in some detail. In the mechanical breakup model, proposed by Norem and his colleagues, the force due to the intense surface field at the tip of a projection exceeds the tensile strength of the metal, causing a fragment of the tip to break loose. Once this micro-particle has separated from the emitter tip, it is subjected to an intense electron bombardment by field emission electrons from the remaining tip. When the gap is comparable to the micro-particle diameter, the power per unit area (gap voltage times the field emission current per unit area) is sufficient to vaporize the micro-particle before it has had time to move away by another micro-particle diameter.

A variation in this scenario assumes that the tip of the emitter begins to melt rather than break off. One might guess that I^2R heating could produce such melting. However, for an emitter tip with any reasonable geometry, diffusion carries away the heat almost as fast as it is produced. This is true even for a tip shaped like a cylinder with a ten to one height/diameter ratio, unless the cylinder has a sub-nanometer diameter. However, a melting model that will work assumes a layer of adsorbed gas (O_2 , CO , etc.) in the area surrounding the emitter, possibly at

a grain boundary. Electron back-bombardment then produces electron-induced desorption of the gas. The gas moves out from the surface to the region of the tip, where field emission electrons ionize it. The ions then move toward the tip, impacting the tip surface and heating it to the melting point.

The two models can be compared with experiment at several points. In the mechanical break-off model at a surface field of 7 GeV/m (the maximum breakdown surface field measured for niobium), the tensile strength of niobium exceeds the E^2 force by a factor of 2.5. However if a chunk of the tip is fractured or loosely attached, it would be easily pulled off at this field level. Note that in this model the breakdown field is independent of the tip area. In the molten liquid droplet model for the tip, a droplet is pulled off when the E^2 force exceeds the restraining force due to surface tension. This occurs at a critical value of the area. In Jens Knobloch's thesis (Cornell university, 1997, Fig. 5.38), starburst formation tends to occur at emitter areas between 10^{-15} and 10^{-16} m², in rough agreement with the value obtained in the liquid droplet model by equating the E^2 force with that due to surface tension. It is likely that both models apply to plasma spot formation on practical structure surfaces.

2. Crater Clustering—a Pre-condition for Surface Melting

Why is crater clustering necessary?

The area around a plasma spot subject to electron back-bombardment is on the

order of 100 μm in diameter. The power per unit area produced by these electrons is simply not enough to raise the surface temperature to the melting point on a 100 ns time scale. What is needed are a large number of closely spaced, active plasma spots within this same area. A crater field, consisting of hundreds of overlapping craters and dozens of plasma alive within the field, is needed to provide sufficient power per unit area to melt the surface.

How do crater clusters form?

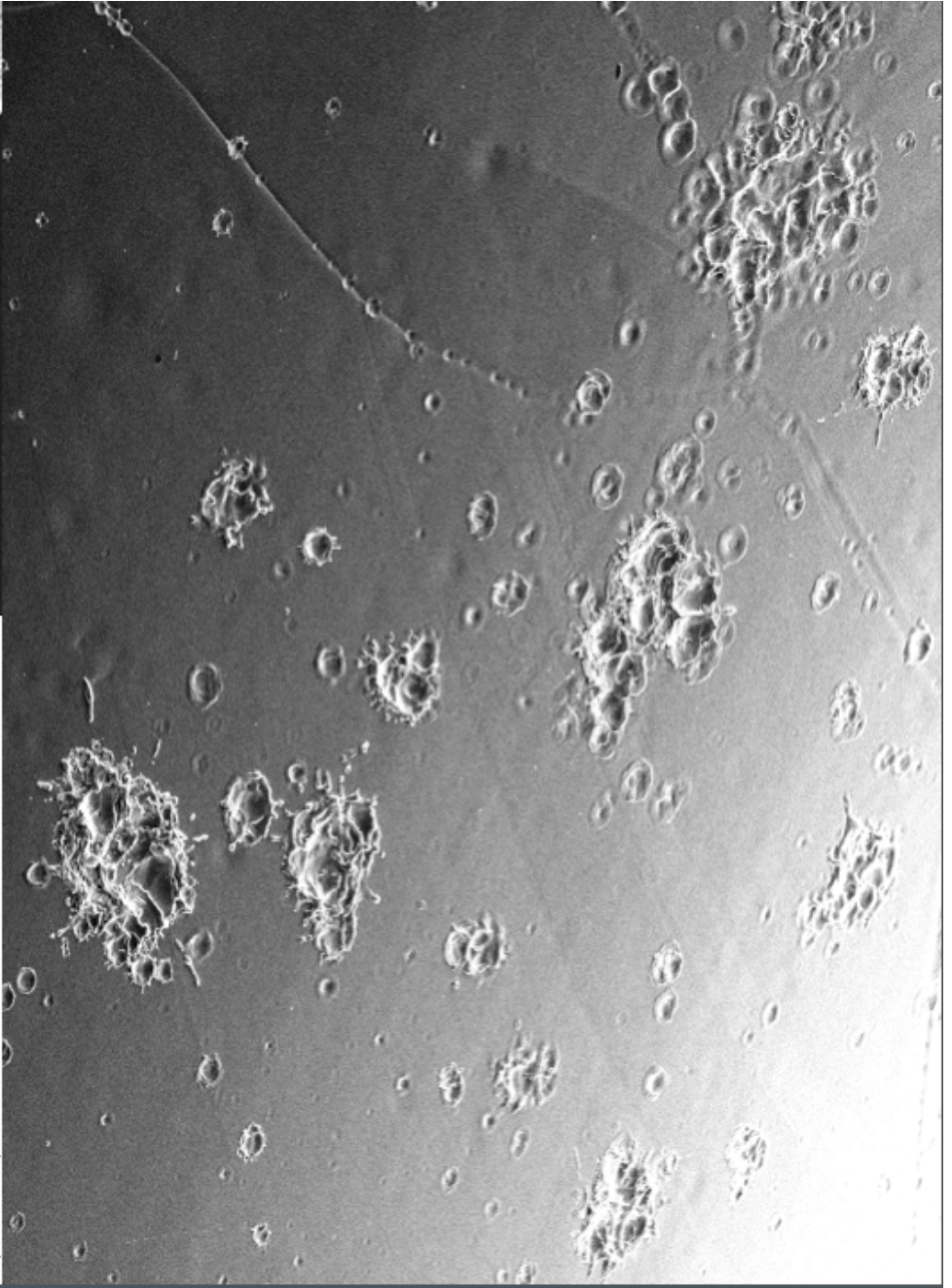
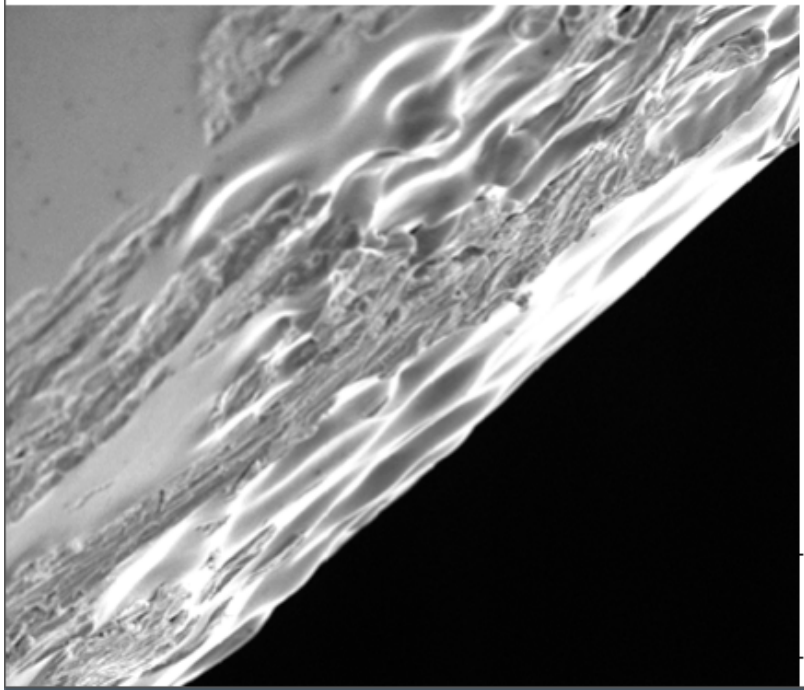
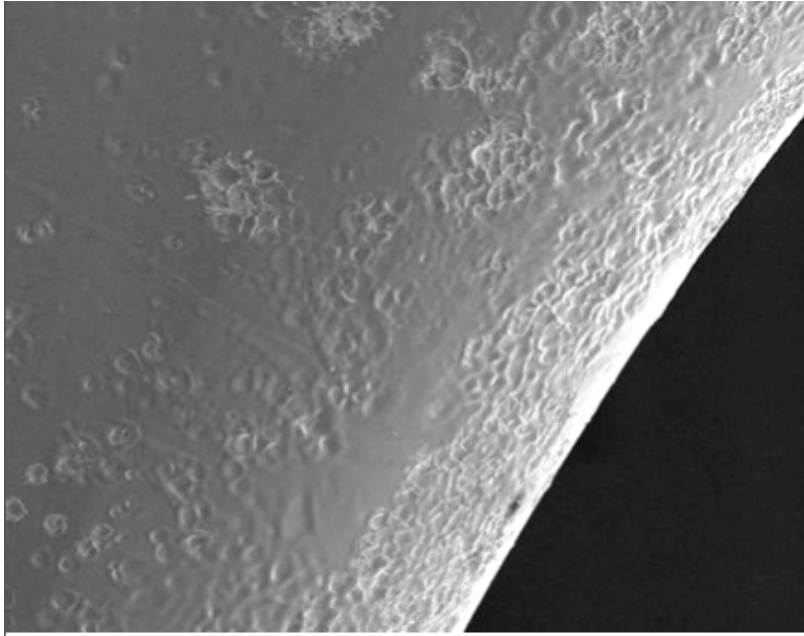
A crater left behind by the destruction of a field emitter looks somewhat like a volcano crater. Material that was thrown or pushed out from the central depression forms a jagged rim surrounding it. The sharply-pointed features on the crater rim can themselves become field emitters. Also, there may be loosely attached debris in high field regions on the crater rim that can readily form plasmas spots following Norem's model. As the sharpest surface features are burned away during processing, it becomes more and more likely that new plasma spots will form on the rim of an existing crater, producing two overlapping craters. The total rim circumference of the two overlapping circular craters is larger (by a factor of $5/3$) than the rim circumference of a single crater, making the probability still higher that a new plasma spot will form on the double crater. As more and more craters are added to the cluster, the probability of a hit continues to increase, although at a decreasing rate per additional crater. In this way clusters of hundreds of overlapping or closely spaced craters can form. Conditions are now ripe for dozens

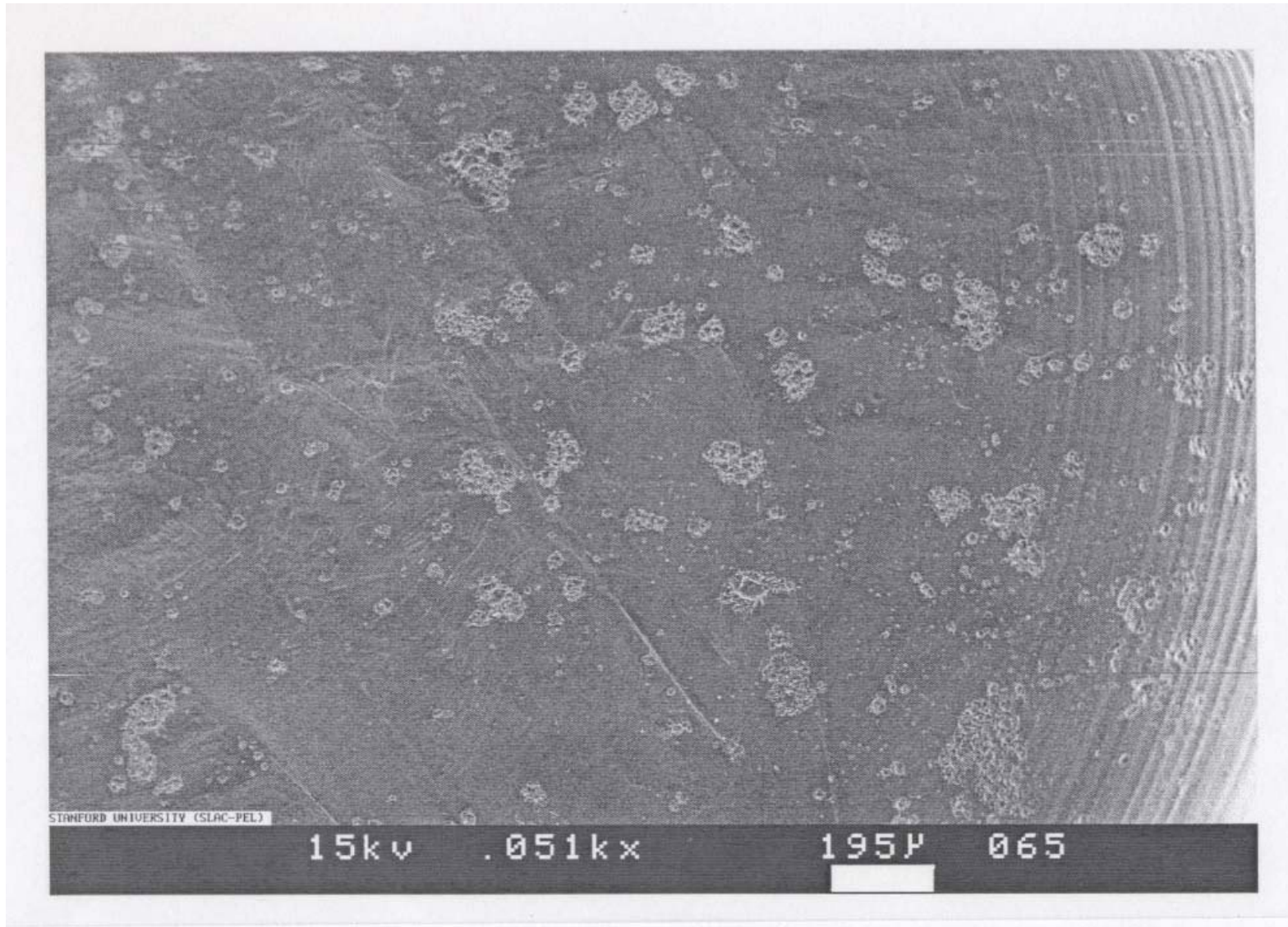
of plasma spots to be alive within the cluster during a time window of 30 ns or so. Electron back-bombardment can now heat the entire cluster area and raise the temperature to the melting point in this time frame.

The photos on the next page (courtesy of Chris Adolphsen, SLAC) of the iris tip region of an iris in a TW accelerator structure illustrate the process. Single isolated craters form in lower field regions away from the iris tip. Closer to the iris tip small crater clusters begin to form, and still closer larger clusters form. Finally, in the tip area itself smooth puddled regions, indicative of melting, are seen.

The process of crater clustering is illustrated even more clearly by the SEM image on p. 8, provided by Lisa Laurent (SLAC). The image shows a surface that has been processed to ~ 500 /m at 150 ns in the Windowtron rf breakdown test apparatus at SLAC (for details see: Lisa Laurent, High Gradient Breakdown Studies, Ph.D. thesis, University of California, Davis, 2002). The high surface field is produced by a 1.4 mm gap between demountable re-entrant electrodes in an X-band klystron-like cavity. The field is nearly uniform over the test surface, in contrast to the images on p.7. As seen in the image, there are numerous isolated single craters, several groups of two to a dozen craters, and about 15 clusters with more than a dozen craters. Clearly, most of the craters on the surface are members of a cluster. There is not enough electron bombardment power available in this particular cavity to melt the surface.

II





SEM image illustrating crater clustering. The copper electrode surface has been processed to ~ 500 MV/m in an X-band cavity (Courtesy of Lisa Laurent, SLAC).

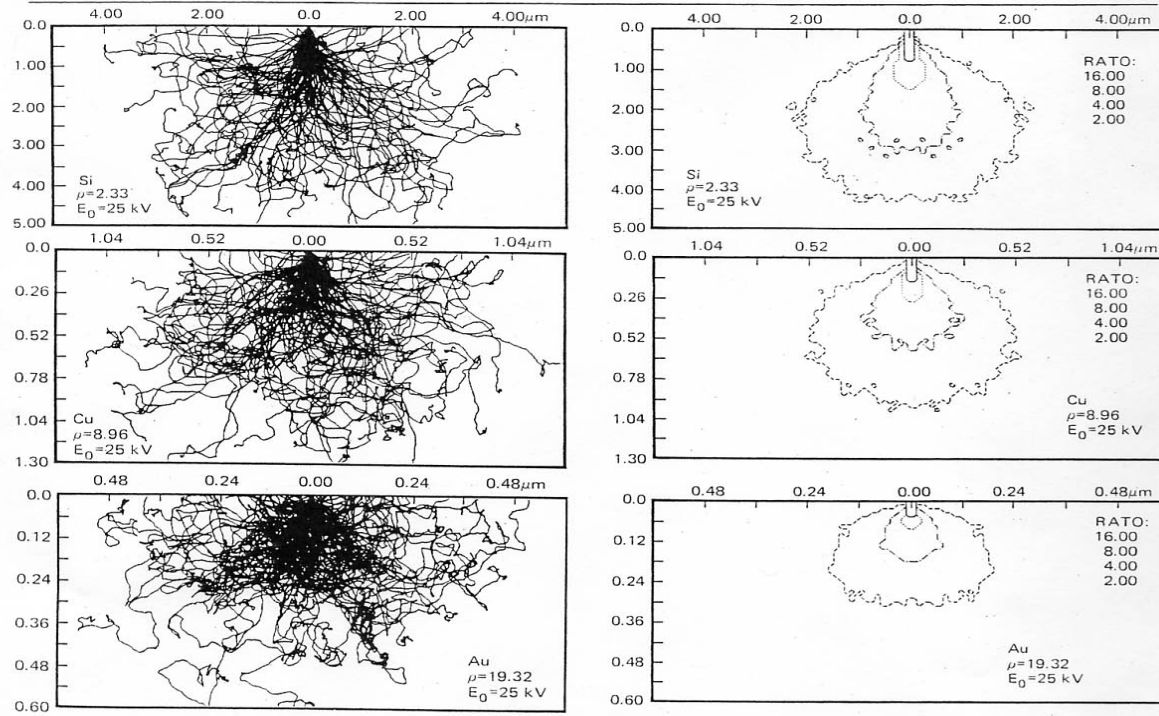
3. Theoretical Prediction for the Threshold Surface Field at Destructive Breakdown for Various Metals

Penetration of electrons into metals

An electron incident on the metal surface will produce a cascade of scattered electrons that will penetrate a considerable distance into the metal. *This distance will depend on the energy of the incident electron and on the density of the metal.* The images on the next page show Monte Carlo simulations for electron scattering and energy dissipation for 25 keV electrons incident on silicon, copper and gold targets [D. F. Keyser, *Scanning electron microscopy/1981/1 pp. 47-62 (SEM Inc. AMF O'Hare, Chicago, IL)*]. Approximate penetration depths of the showers in microns are given in the table below, along with the densities of these metals.

<u>Penetration Depth X_0 (μm)</u>	<u>Density ρ (g/cm^3)</u>	<u>$X_0\rho$</u>
Si	2.2	5.1
Cu	0.59	5.3
Au	0.25	4.8

For a wide range of materials, the product of the penetration depth and the density is roughly constant. As a function of incident electron energy, the penetration depth varies approximately as $X_0 \sim V^{1.5}$ in the energy range of interest.



Knowing the deposition of energy as function of depth and radial position from these Monte Carlo simulations, the surface temperature as a function of time can be computed from a solution of the 2D heat diffusion equation. However, an approximate solution can be obtained fairly easily from a 1D heat diffusion equation.

Calculation of the Temperature Rise at a Metal Surface Subjected to Electron Bombardment

Assumptions

We make these approximations:

- 1. The electron trajectories are normal to the surface and the reflection coefficient is independent of surface material.*
- 2. The energy is deposited uniformly over the penetration depth.*
- 3. All the incident electrons have the same energy.*

Parameters and definitions

P_A (W/cm^2): Incident power per unit area

X_0 (cm): Penetration depth

C_s ($\text{K} (\text{W}/\text{cm}-^\circ\text{C})$): Thermal conductivity

T ($^\circ\text{C}$): Surface temperature increase above 20°C

D (cm²/s): Diffusivity. $D = K/C_s\rho$ T_m (°C): Melting point

X_D (cm): Diffusion depth. $X_D = (Dt)^{1/2}$ H (J/g): Heat of fusion

Limits with simple solutions for the surface temperature rise

1. Penetration depth large compared to the diffusion depth

$$T = P_A t / (X_0 \rho C_s) \sim P_A t / C_s \quad (X_0 \rho \cong \text{constant})$$

2. Penetration depth small compared to the diffusion depth

$$T = P_A (2/\pi^{1/2}) X_D / K \sim P_A t^{1/2} (D/K)^{1/2}$$

Solution for the general case at time t_0

$$T = \frac{P_A}{X_0 C_s \rho} \int_0^{t_0} \text{erf} \left\{ \frac{X_0}{[4D(t_0 - t)]^{1/2}} \right\} dt$$

Recalling that $X_0 \rho$ is approximately constant, the power per unit area at $T = T_m$ is

proportional to

$$P_A \sim T_m C_s / I$$

where $I(t_0)$ is the integral in the preceding equation.

We will want to melt the surface at the beginning of the rf pulse in a time which is a reasonably short fraction of the total pulse length. The main part of the pulse can then be spent in developing the geometric features discussed in Sec. 4. Assuming a total X-band pulse length in the range 100–400 ns, we'll somewhat arbitrarily pick $t_0 = 30$ ns. The breakdown field scales as $(P_A)^{1/2}$ giving

$$E_b \sim \left[\frac{T_M C_S}{I(30ns)} \right]^{1/2} .$$

However, after the temperature is raised to the melting point, additional energy (the heat of fusion) must be applied to liquefy the metal. Consider the element of depth dx closest to the surface just as the surface reaches the melting point. As additional energy is supplied, the temperature of the metal in dx can no longer change, nor that of its neighboring element of material. Therefore, there is no temperature gradient close to the surface and the additional energy required to melt the material can be calculated without taking heat diffusion into account. Including the heat of fusion, the breakdown field scaling becomes

$$E_b \sim \left[\frac{T_m C_s}{(I/t_0)} + H \right]^{1/2} .$$

The dimensionless factor I/t_0 depends on the ratio of X_0/X_D . If this ratio is large, $I/t_0 \rightarrow 1$. If it is small, the first term in the brackets reduces to the correct value for diffusive heat flow.

One further simplification can be made. In standard texts on thermal physics [e.g., Reif, *Fundamentals of Statistical and Thermal Physics (Mcgraw-Hill, 1965)*] it is shown that **the product of the specific heat and the atomic weight of a metal is approximately constant**. Except for a few metals (e.g., beryllium) the constant is 24 J/g \pm 6%. In this approximation, $T_m C_s$ in the expression above can be replaced by 24 T_m/A .

The results of the calculation are given in the table on the next page. The normalized breakdown fields seem to fall into several well-defined groups, with gaps in between. Beryllium is clearly the all-star metal, although safety issues make it awkward to work with. The metals shown in red give substantial breakdown field improvement factors (in the range 1.3–1.4), and several of them are quite practical to work with. Perhaps the most interesting material of all is carbon. There are at least two possible ways to obtain an iris tip with a carbon surface. First, an iris-tip ring can be machined from graphite. Because carbon is slightly conducting, the perimeter of the central hole in the ring can be

Breakdown fields normalized to copper for various metals

1.0 — 1.13		1.19 — 1.23		1.28 — 1.42	
Cu	1.00	Ni	1.19	Mo	1.28
Ta	1.00	Fe	1.19	Ti	1.32
Tc	1.02	W	1.20	Sc	1.35
Ir	1.02	SS	1.21	Cr	1.39
Zr	1.06	Nb	1.21	V	1.42
Ca	1.06	Al	1.21		
Rh	1.07	Ru	1.22		
Y	1.09	Mg	1.23		
Os	1.10	Co	1.23		
Mn	1.12				

Superstar

Be 2.53

Non-metals

B 2.53

C ~ 4

electroplated with copper, and this insert then brazed onto the body of the iris. Second, at this Workshop Euclid Techlabs LLC has shown that chemical vapor deposition of a layer of diamond is also a possibility. On the next page the above breakdown field groups are shown on the Periodic Table of the Elements.

Periodic table of the elements

Period	Group Ia	Group IIa	Group IIIa	Group IVa	Group Va	Group VIa	Group VIIa	Group VIII	Group Ib	Group IIb	Group IIIb	Group IVb	Group Vb	Group VIb	Group VIIb	Inert Gases		
1	1.008 H ₁														1.008 H ₁	4.003 He ₂		
2	6.94 Li ₃ FR	9.01 Be ₄ FSWR									10.81 B ₅ MP	12.01 C ₆ FSRQ	14.01 N ₇	16.00 O ₈	19.00 F ₉	20.18 Ne ₁₀		
3	22.99 Na ₁₁	24.31 Mg ₁₂ FSWRP XZ	Transition Elements								26.98 Al ₁₃ MFSWR PTXZH	28.09 Si ₁₄ SPL Z	30.97 P ₁₅	32.06 S ₁₆	35.45 Cl ₁₇	39.95 Ar ₁₈		
4	39.10 K ₁₉	40.08 Ca ₂₀ ★Z	44.96 Sc ₂₁ FWP	47.90 Ti ₂₂ MFSWRP TX	50.94 V ₂₃ MFSWR PXZ	52.00 Cr ₂₄ MFSWP Z	54.94 Mn ₂₅ MFP	55.85 Fe ₂₆ MFSWR PTX	58.93 Co ₂₇ MFSWR PZ	58.71 Ni ₂₈ MFSWR PTXZ	63.55 Cu ₂₉ MFSWR PTXZ	65.38 Zn ₃₀ FSWRP XZ	69.72 Ga ₃₁ ★Z	72.59 Ge ₃₂ L	74.92 As ₃₃ L	78.96 Se ₃₄ L	79.90 Br ₃₅ L	83.80 Kr ₃₆
5	85.47 Rb ₃₇	87.62 Sr ₃₈ ★	88.91 Y ₃₉ FRPW	91.22 Zr ₄₀ MFSWR PTX	92.91 Nb ₄₁ MFSWR PTXZ	95.94 Mo ₄₂ MFSWR PTXZ	98.91 Tc ₄₃	101.07 Ru ₄₄ MP	102.91 Rh ₄₅ MFWP	106.4 Pd ₄₆ MFWPT	107.87 Ag ₄₇ MFSWR PT	112.40 Cd ₄₈ MFSWR LZ	114.82 In ₄₉ MFSWR P	118.69 Sn ₅₀ MFSWR PX	121.75 Sb ₅₁ FPL	127.60 Te ₅₂ L	126.90 I ₅₃	131.30 Xe ₅₄
6	132.91 Cs ₅₅	137.34 Ba ₅₆ ★	138.91 La ₅₇ FSWRP	178.49 Hf ₇₂ MFSWR P	180.95 Ta ₇₃ MFSWR PTXZ	183.85 W ₇₄ MFSWR PXZ	186.2 Re ₇₅ MFWP	190.2 Os ₇₆	192.22 Ir ₇₇ MFWP	195.09 Pt ₇₈ MFWPT	196.97 Au ₇₉ MFWPT	200.59 Hg ₈₀	204.37 Tl ₈₁ FRW	207.19 Pb ₈₂ MFSWR PXZ	208.98 Bi ₈₃ FPR	209 Po ₈₄	210 At ₈₅	222 Rn ₈₆
7	223 Fr ₈₇	226.03 Ra ₈₈	227 Ac ₈₉	261 (Rf) ₁₀₄	262 (Ha) ₁₀₅	Metals available from  Goodfellow are in the white boxes												

Key

Atomic weight
Alloys ● Compounds ★
Symbol and atomic number
M Microfoil F Foil K Flake
S Sheets (> 0.5 mm) Q Fabric
W Wire R Rod P Powder
L Lumps T Tube H Honeycomb
X Sputtering Targets Z Single Crystal
Note: Atomic weights shown as integers are for the most stable isotope of the element

47.90 ● ★ Ti ₂₂ MFSWRP TX
--

Lanthanides (rare earths)	140.12 Ce ₅₈ FWRP	140.91 Pr ₅₉ FWRP	144.24 Nd ₆₀ FWRP	145 Pm ₆₁	150.35 Sm ₆₂ FRP	151.96 Eu ₆₃ FWP	157.25 Gd ₆₄ FWRP	158.93 Tb ₆₅ FWRP	162.50 Dy ₆₆ FWRP	164.93 Ho ₆₇ FWRP	167.26 Er ₆₈ FWRP	168.93 Tm ₆₉ FP	173.04 Yb ₇₀ FWRP	174.97 Lu ₇₁ FP
Actinides	232.04 Th ₉₀ FW	231.04 Pa ₉₁	238.03 U ₉₂ FW	237.05 Np ₉₃	244 Pu ₉₄	243 Am ₉₅	247 Cm ₉₆	247 Bk ₉₇	251 Cf ₉₈	254 Es ₉₉	257 Fm ₁₀₀	258 Md ₁₀₁	259 No ₁₀₂	260 Lw ₁₀₃

Breakdown Fields Normalized to Copper for Various Materials

1.0—1.13  1.19—1.23  1.28—1.42  2.20 (Be) 

Non-metals: B = 2.53 C ~ 4 

4. From Surface Melting to Destructive Breakdown

Some Comments on the Properties of Destructive Breakdown

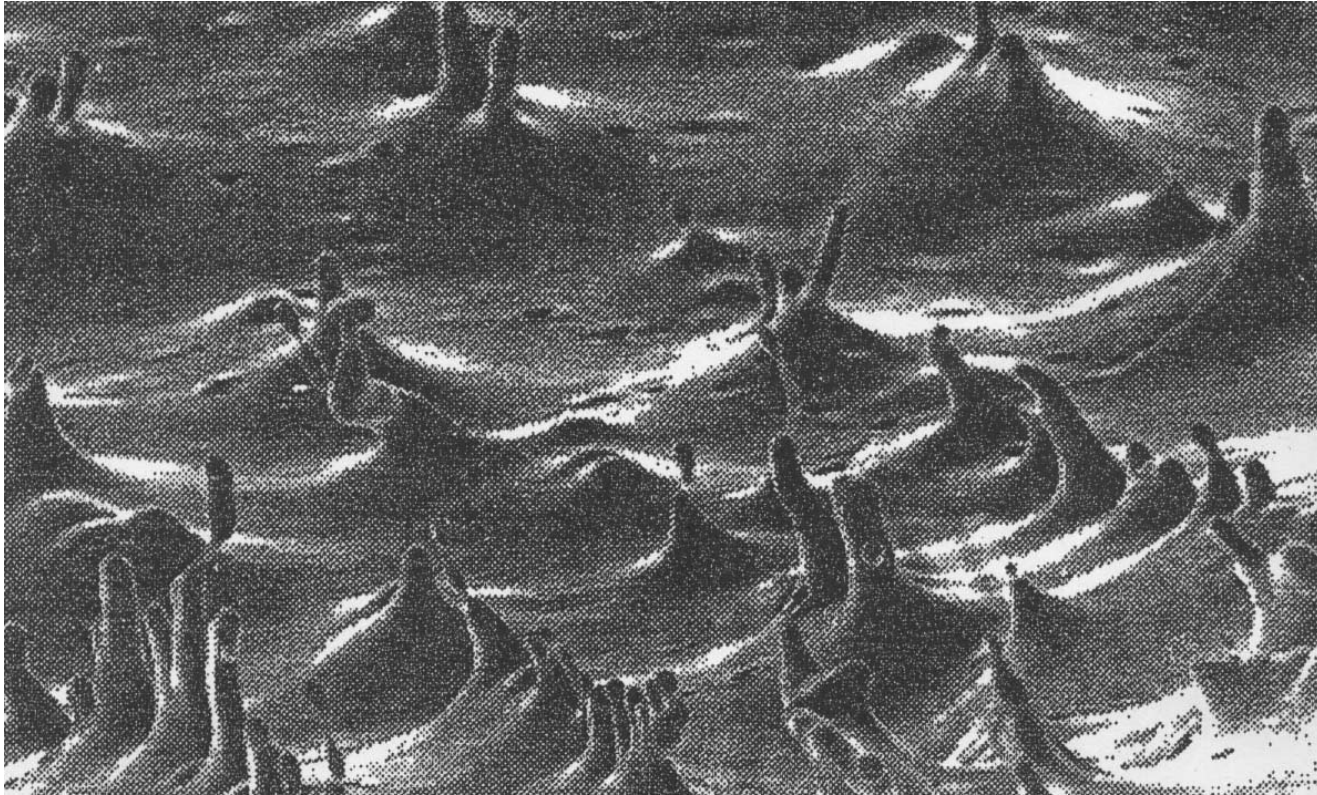
Destructive breakdown forms an absolute limit on gradient.

At this limit, macroscopic amounts of material are removed or displaced, i.e., the shape of an iris tip can be deformed without actual material removal.

Measurements show that the threshold for catastrophic breakdown varies with pulse length as $1/(T_p)^{1/4}$ (Dolgashev and Tantawi).

To first order, the threshold for destructive breakdown at the same pulse length for structures with the same geometry seems to be roughly independent of frequency for frequencies that are sufficiently high, although the experimental evidence for this is not yet conclusive. In this limit breakdown is a single surface phenomenon—the physics during the initial stage of destructive breakdown is independent of distant surfaces. The extent of the final-stage damage does of course depend on the energy available in a structure cell.

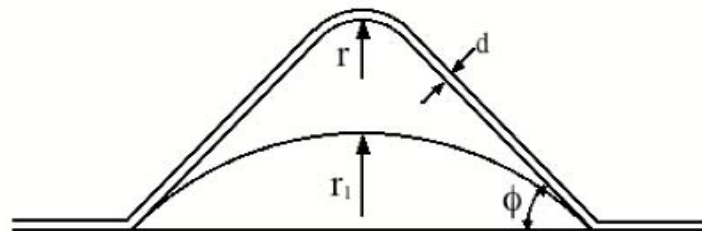
Next, lets look at a photo of a metal surface that has been raised to the melting point in an intense dc electric field (next page).



Note the pyramid-like features with a base angle of about 45° , with finger-like projections emerging from the apex of almost every pyramid. It is reasonable to assume that similar effects will take place for a molten surface in an rf field. Of course, starting with a relatively flat surface, material must be moved around mechanically—a slow process such that not much can happen during a

sub-microsecond pulse. It will therefore take many such pulses to build up features like those shown above. As a first step, let's build a theory for how these pyramids with projections jutting from their tops might form. We'll find that these features have a relationship to Kevlar bullet-proof vests and to some work in 1964 by Geoffrey Taylor on the disintegration of water drops at the tip of a capillary in an electric field.

Theory for pyramid (cone) growth with subsequent apex instability (see SLAC-PUB-11086 for details)



The figure above models the growth of the pyramid. We assume that growth starts from a shallow, rounded perturbation on the molten surface with radius r_1 . The surface field is enhanced at the apex of the perturbation, producing a pressure difference between the apex and the base. This “ponderomotive” force pulls liquid metal toward the apex, causing the perturbation to grow. After the feature has

grown a bit, the apex must have a roughly spherical shape. This is so because, since it's a liquid, it must be in hydrostatic equilibrium; that is, the external force (proportional to $r^2 E_S^2$) pulling on the surface must be balanced by the surface tension pulling on the perimeter $2\pi r$. The resulting expression for the radius is

$$r = 8\alpha/\epsilon_0 E_S^2,$$

where α is the surface tension (1.4 Nt/m for molten copper).

As the height of the cone increases the radius of the cap decreases and the surface field E_S and enhancement factor $\beta = E_S/E_0$ also increases. Simulations show that beta can be modeled as $\beta \sim r^{-n}$, where n is a function of the base angle ϕ . For the molten cap to be in hydrostatic equilibrium, the radius must vary as $r/r_1 = E_1^2/E_S^2$, giving $\beta = \beta_1 (r/r_1)^{-1/2}$, where β_1 is the value of beta at $r = r_1$. Simulations show that for n to be exactly 1/2 the base angle ϕ must be 41° with $\beta_1 = 1.90$. This is in agreement with some 1964 work by Taylor on a water droplet at the tip of a capillary exposed to an electric field (Geoffrey Taylor, Disintegration of Water Drops in an Electric Field (*Proc. Roy. Soc. A, Vol. 280, pp. 383-397*). Some results are shown on the next page.

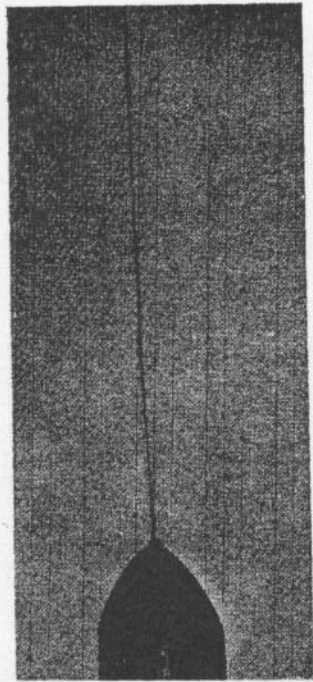
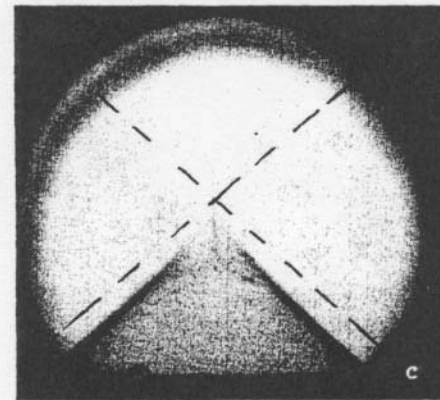
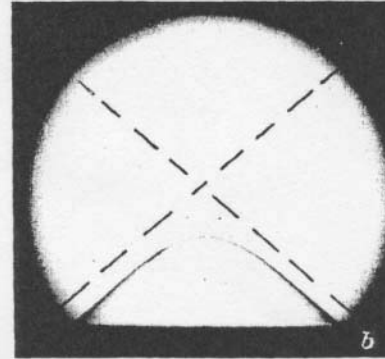
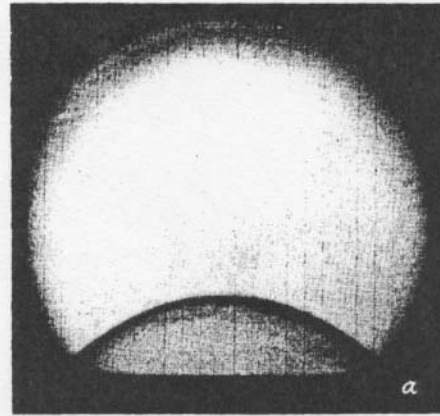


FIGURE 1



As the electric field is increased (*a* through *c* above), the radius at the tip of the droplet decreases until an unstable point is reached. A jet of liquid is then seen shooting out from the tip (inset at the left). At the point of the instability, the base angle of the pyramid in *c* is 40.7°. A search of the literature on hydrodynamics will probably uncover the physics underlying this instability (Taylor instability?), and the critical value of the tip radius at which it occurs.

We next develop a model for the growth of the cone height with time. Assume a layer of molten metal of thickness *d* on the sides of the cone. The electric field pulling on the liquid surface increases from the bottom to the top of the cone—that is, there is an increasing negative pressure from bottom to top in the liquid layer. The liquid, flowing in the direction of lower internal pressure, then moves toward the top of the cone. A force of this type is often termed a ponderomotive force. The average flow velocity of the material is calculated to be $v = \epsilon_0 E_s^2 d / 8\eta$, where η is the viscosity. This can, in turn, be converted to a growth rate in cone height and hence in β . After a little algebra, we obtain

$$\beta = \frac{2}{[1 - BE_s^4 T]^{1/6}}$$

where $B \approx 6d^2 \epsilon_0^2 / \alpha \eta r_1$ and *T* is the integrated time (repetition rate times the pulse length, with an initial melting time ~ 30 ns subtracted). Note that $E_0^4 T$ is a constant

at the singularity, in agreement with experiment [V. Dolgashev and S. G. Tantawi, RF Breakdown in X-band Waveguide, *EPAC 2002 (also SLAC-PUB-10355)*]. The details of the model could vary a bit, but the scaling $E_S^4 T_P = \text{constant}$ is robust.

Oh yes—bullet-proof vests. Kevlar is made by exposing a molten layer of polymer on a metal plate to a strong electric field. As the field is increased, long strings of liquid with diameters ~ 10 nm suddenly emerge from the liquid surface (we'll postulate that the formation of these liquid strings follows the model illustrated on p. 19). The liquid strings cross the voltage gap and are laid down on a condensing plate in a random criss-cross pattern. Layers of these nano-fibers form a cloth (Kevlar) with outstanding mechanical strength.

A Concluding Comment

The model presented here deals only with the ultimate surface field that can be reached on an iris tip without irreversible damage. The extent of the damage will depend on the rf energy available to feed the surface plasma covering the molten region, and this in turn depends on the global properties of the structure. In a real machine where a long structure life is required, one would want to allow an adequate overhead between the operating and the ultimate gradients. In this case a low breakdown probability is a necessity (these breakdowns are of the non-damaging kind that occur during processing). The present model has nothing to

say about the probability for the occurrence of such breakdowns. My own guess is that field emitters are destroyed by melting due to ion bombardment beneath a plasma spot. In this case the temperature rise follows case 2 on p.12. From this the amount of energy per pulse needed to destroy an emitter can be worked out. This energy per pulse is certainly related to the difficulty of processing a particular metal, and probably also to the breakdown rate as a function of pulse energy. Work is continuing on this problem.